Trial Support & Data Analysis for 2015 ONR Sea-Trial
Final Report

Chad M. Smith
The Pennsylvania State University
Applied Research Laboratory
P.O. Box 30
State College, PA 16804-0030
phone: (814) 863-4159 fax: (814) 863-8783 email: cms561@arl.psu.edu

Award Number: N00014-16-1-2490

LONG-TERM GOALS

- Improve the physical understanding and modeling capabilities of shallow-water scattering, clutter, and environmental uncertainty affecting sonar systems and aid in its mitigation.
- Develop traditional and cardioid line-array based processing techniques for scattering, clutter, and environmental assessment.
- Maintain and operate the Five Octave Research Array (FORA) at the direction of ONR-32 to support ONR goals.

OBJECTIVES

This work had two primary tasks. The first was the support of the PI and Penn State Applied Research Laboratory (PSU-ARL) technicians for demobilization and post-experimental cleanup of the FORA acquisition system. This work is in connection with the initial experimental effort of the Littoral Continuous Active Sonar (LCAS) Multi-National Joint Research Project (MN-JRP), which took place off the coast of La Spezia, Italy in late 2015. The second objective is support of the PI and John Preston (now emeritus faculty at PSU-ARL) to process select FORA cardioid data from the LCAS 2015 trial and statistically characterize reverberation and clutter using K-distribution estimates and correlation statistics to aid in Continuous Active Sonar (CAS) and pulsed active sonar (PAS) comparisons.

APPROACH

CAS is a promising new technique to improve sonar performance using high duty-cycle signals. The prior mentioned MN-JRP was designed to explore many aspects of CAS performance and capabilities. This work was designed to support FORA data collection for the MN-JRP experimental effort, as well as aid in processing comparisons of CAS and PAS. The PSU-ARL team was tasked with FORA data collection, demobilization and cleanup of FORA system, as well as characterization of returns from aggregations of fish and other clutter events using acoustic intensity distribution and correlation statistics. Spatial correlation statistics in particular are of prime focus in this research.

Previous work by John Preston, Doug Abraham, Anthony Lyons, and others has shown that K-distribution shape parameter of backscatter from fish schools and clutter events can often be significantly different than that from seafloor and basin boundaries. It has also shown that K-distribution shape parameter can be used as a metric of significantly non-Rayleigh returns from target

REPORT DOCUMENTATION PAGE

Form Approved
OMB No. 0704-0188

1. REPORT DATE *(DD-MM-YYYY)*	2. REPORT TYPE	3. DATES COVERED *(From - To)*
06/21/2017	Final	05/01/2016 through 05/01/2017

4. TITLE AND SUBTITLE
Trial Support & Data Analysis for 2015 ONR Sea-Trial

5a. CONTRACT NUMBER

5b. GRANT NUMBER
N00014-16-1-2490

5c. PROGRAM ELEMENT NUMBER

6. AUTHOR(S)
Chad Smith

5d. PROJECT NUMBER
24674

5e. TASK NUMBER

5f. WORK UNIT NUMBER

7. PERFORMING ORGANIZATION NAME(S) AND ADDRESS(ES)
The Pennsylvania State University Applied Research Labotatory
Office of Sponsored Programs
110 Technology Center Building
University Park, PA 16802-7000

8. PERFORMING ORGANIZATION REPORT NUMBER

9. SPONSORING/MONITORING AGENCY NAME(S) AND ADDRESS(ES)
Office of Naval Research
875 North Randolph Street
Arlington, VA 22203-1995

10. SPONSOR/MONITOR'S ACRONYM(S)

11. SPONSORING/MONITORING AGENCY REPORT NUMBER

12. DISTRIBUTION AVAILABILITY STATEMENT
Approved for Public Release, distribution unlimited

13. SUPPLEMENTARY NOTES

14. ABSTRACT
This work had two primary tasks. The first was the support of the PI and Penn State Applied Research Laboratory (PSU-ARL) technicians for demobilization and post-experimental cleanup of the FORA acquisition system. This work is in connection with the initial experimental effort of the Littoral Continuous Active Sonar (LCAS) Multi-National Joint Research Project (MN-JRP), which took place off the coast of La Spezia, Italy in late 2015. The second objective is support of the PI and John Preston (now emeritus faculty at PSU-ARL) to process select FORA cardioid data from the LCAS 2015 trial and statistically characterize reverberation and clutter using K-distribution estimates and correlation statistics to aid in Continuous Active Sonar (CAS) and pulsed active sonar (PAS) comparisons.

15. SUBJECT TERMS

16. SECURITY CLASSIFICATION OF:			17. LIMITATION OF ABSTRACT	18. NUMBER OF PAGES	19a. NAME OF RESPONSIBLE PERSON
a. REPORT	b. ABSTRACT	c. THIS PAGE	U	14	Chad Smith
u	u	u			19b. TELEPONE NUMBER (*Include area code*) 814-863-4159

INSTRUCTIONS FOR COMPLETING SF 298

1. REPORT DATE. Full publication date, including day, month, if available. Must cite at lest the year and be Year 2000 compliant, e.g., 30-06-1998; xx-08-1998; xx-xx-1998.

2. REPORT TYPE. State the type of report, such as final, technical, interim, memorandum, master's thesis, progress, quarterly, research, special, group study, etc.

3. DATES COVERED. Indicate the time during which the work was performed and the report was written, e.g., Jun 1997 - Jun 1998; 1-10 Jun 1996; May - Nov 1998; Nov 1998.

4. TITLE. Enter title and subtitle with volume number and part number, if applicable. On classified documents, enter the title classification in parentheses.

5a. CONTRACT NUMBER. Enter all contract numbers as they appear in the report, e.g. F33615-86-C-5169.

5b. GRANT NUMBER. Enter all grant numbers as they appear in the report, e.g. 1F665702D1257.

5c. PROGRAM ELEMENT NUMBER. Enter all program element numbers as they appear in the report, e.g. AFOSR-82-1234.

5d. PROJECT NUMBER. Enter al project numbers as they appear in the report, e.g. 1F665702D1257; ILIR.

5e. TASK NUMBER. Enter all task numbers as they appear in the report, e.g. 05; RF0330201; T4112.

5f. WORK UNIT NUMBER. Enter all work unit numbers as they appear in the report, e.g. 001; AFAPL30480105.

6. AUTHOR(S). Enter name(s) of person(s) responsible for writing the report, performing the research, or credited with the content of the report. The form of entry is the last name, first name, middle initial, and additional qualifiers separated by commas, e.g. Smith, Richard, Jr.

7. PERFORMING ORGANIZATION NAME(S) AND ADDRESS(ES). Self-explanatory.

8. PERFORMING ORGANIZATION REPORT NUMBER. Enter all unique alphanumeric report numbers assigned by the performing organization, e.g. BRL-1234; AFWL-TR-85-4017-Vol-21-PT-2.

9. SPONSORING/MONITORS AGENCY NAME(S) AND ADDRESS(ES). Enter the name and address of the organization(s) financially responsible for and monitoring the work.

10. SPONSOR/MONITOR'S ACRONYM(S). Enter, if available, e.g. BRL, ARDEC, NADC.

11. SPONSOR/MONITOR'S REPORT NUMBER(S). Enter report number as assigned by the sponsoring/ monitoring agency, if available, e.g. BRL-TR-829; -215.

12. DISTRIBUTION/AVAILABILITY STATEMENT. Use agency-mandated availability statements to indicate the public availability or distribution limitations of the report. If additional limitations/restrictions or special markings are indicated, follow agency authorization procedures, e.g. RD/FRD, PROPIN, ITAR, etc. Include copyright information.

13. SUPPLEMENTARY NOTES. Enter information not included elsewhere such as: prepared in cooperation with; translation of; report supersedes; old edition number, etc.

14. ABSTRACT. A brief (approximately 200 words) factual summary of the most significant information.

15. SUBJECT TERMS. Key words or phrases identifying major concepts in the report.

16. SECURITY CLASSIFICATION. Enter security classification in accordance with security classification regulations, e.g. U, C, S, etc. If this form contains classified information, stamp classification level on the top and bottom of this page.

17. LIMITATION OF ABSTRACT. This block must be completed to assign a distribution limitation to the abstract. Enter UU (Unclassified Unlimited) or SAR (Same as Report). An entry in this block is necessary if the abstract is to be limited.

and clutter events. In this work, the PI and John Preston performed analysis on data taken using the FORA acquisition system during the 2015 LCAS experiment to statistically characterize scattering from an ideal target as well as biologic and bottom clutter. Due to the distributions relatively common use and large body of related literature, K-distribution shape parameter estimates were used as a metric of the Rayleigh-like nature of backscattered returns. This metric was then compared with the estimated spatial correlation function and aperture coherence in order to determine the extent of additional information which can be gleaned from using spatial correlation information in addition to commonly used intensity distributions (such as the K-distribution) in sonar signal processing. The spatial correlation coefficient (normalized cross-correlation), ρ, was chosen as the primary metric for this comparison,

$$\rho(\Delta x) = \frac{\langle p^*(x)\, p(x+\Delta x)\rangle}{\sqrt{\langle p^*(x)\, p(x)\rangle \langle p^*(x+\Delta x)\, p(x+\Delta x)\rangle}} \qquad \text{(Eq. 1)}$$

where, Δx , is the displacement distance between spatially separated receiver elements. The mean of the correlation coefficient over all displacement distances (unique receiver spacings) across the array aperture,

$$AC = \frac{1}{N}\sum_{j}^{N} \rho(\Delta x_j) \qquad \text{(Eq. 2)}$$

will be referred to as the aperture coherence or AC. N is the number of unique receiver spacings for a given array.

The normalized cross-correlation is commonly used as a metric of the spatial coherence between two points in space,[6,7] and although this metric can be difficult to physically interpret due to the non-unique dependence of the correlation coefficient on physical scattering processes, this work aimed to determine if this metric can provided additional information about the physical characteristics of acoustic clutter or target events compared to commonly used intensity distributions. Figure 1 is a schematic of the spatial correlation of a scattered field measured between two separated points in space. The correlation coefficient is a normalized measure of the linear relationship between the signals received at each receiver. The upper portion of Figure 1 shows two closely spaced receivers and the corresponding high correlation coefficient (0.9 in this example) found along the spatial correlation surface to the left. The lower plot in this figure shows how the correlation coefficient will typically drop as the receivers are moved farther from one another. It can be shown that the shape of this curve is closely related to transmitter and receiver beampatterns assuming a distributed random-phase point-scatterer field.[4] However, clutter and targets events generally defy this assumption and may impact the general shape of this curve.

Brown et al.[3] points out that coherent backscatter is generally associated with smooth surfaces of finite size and is often broadly spatially coherent, while incoherent backscatter is often associated with rough surface scattering and is more narrowly spatially coherent. Jackson and Moravan[4] discuss the dependence of horizontal correlation on beampattern based upon a point scattering model and show noticeable differences in boundary and volume reverberation also using this model. In this work we verify that clutter from volume scattering (biologics), stationary bottom clutter, and ideal targets do indeed have measureable changes in coherence characteristics that may be used for the purpose of classification in long-range sonar systems. It was expected (and determined) that both the K-distribution shape parameter and correlation statistics can provide an estimate of the Rayleigh-like or non-Rayleigh-like nature of acoustic returns. In other words, changes in both the K-distribution shape

parameter as well as the aperture coherence may be used to detect and classify target and clutter events. However, because distribution statistics provide a classifier using only time domain information and aperture correlation is a statistical comparison of the signal variance over space, these two metrics may provide very different information about the scattered field and in turn the scatterer geometry. This work investigates this thesis to determine if the two metrics may have complementary or simply duplicative classification information.

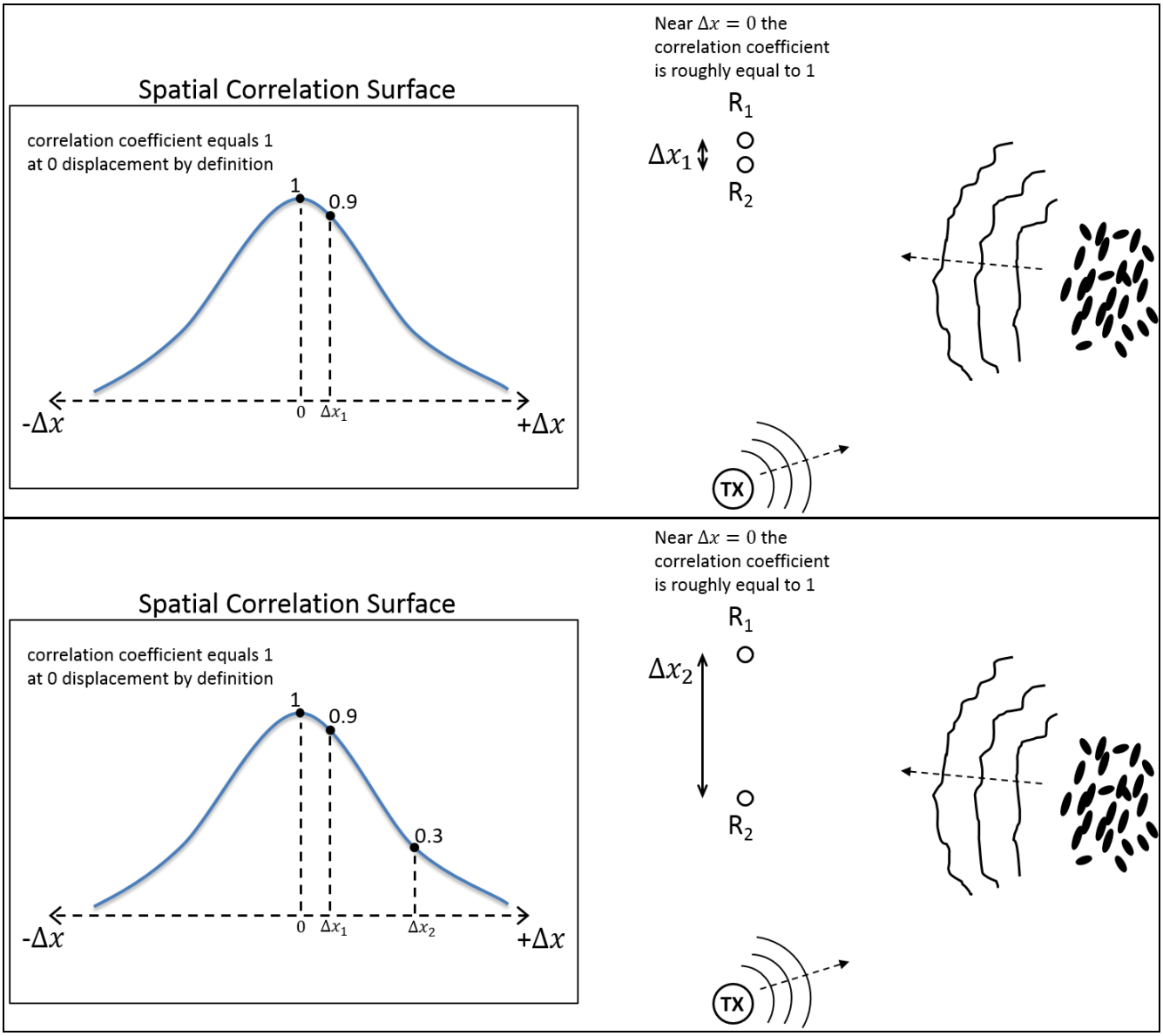

Figure 1: Schematic showing a diagram of the spatial correlation surface of the backscattered field. The correlation coefficient is a normalized measure of the linear relationship between the signals received at the two locations in space. The upper portion of this figure shows two closely spaced receivers and the corresponding high correlation coefficient (0.9 in this example) along the spatial correlation surface to the left. The lower portion of this figure then shows how the correlation coefficient will drop off as the receivers are moved farther from one another. It can be shown that the mean shape of this curve is closely related to transmitter and receiver beampatterns assuming a randomly distributed point-scattering field. However, targets and clutter events can defy these assumptions and impact the general shape of this curve.

Polar plots of match filtered return level vs. geographic location were used to locate clutter events and choose data segments for further processing. Match filtered data was range-normalized to remove propagation biases (normalization algorithm from Dale Ellis at DRDC) and more clearly show target and clutter events. K-distribution shape parameter estimates (processing code from D. Abraham) were then performed on select PAS and CAS data segments. The spatial correlation statistics of these data segments was also analyzed and interpolated to similar geographic locations for comparison to K-distribution statistics.

In order to estimate the spatial correlation and aperture coherence across the face of the FORA line array, sub-aperture processing was performed. The FORA cardioid was broken in 32 sub-apertures along the length of the array and each shortened cardioid sub-aperture was beamformed separately and the correlation coefficient (Eq. 1) was calculated between sub-apertures at similar steering angle and range. This provides estimates of the backscattered signal correlation at the displacement distance between the two sub-aperture centers. Figure 2 provides a schematic of this processing method geometry. Note that in the far field the beampatterns of all sub-apertures are looking at largely the same region.

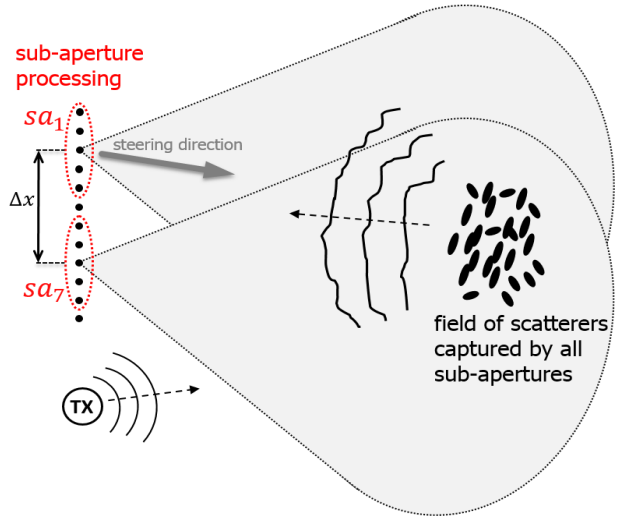

Figure 2: Schematic showing the concept of sub-aperture cardioid processing. This figure shows a short 12 element array (individual cardioid elements are not shown) broken into 8, 5-element sub-apertures. Each sub-aperture is beamformed separately and then the correlation coefficient between sub-apertures is calculated for each displacement distance. This allows the estimation of the spatial correlation surface of backscatter from specific range and azimuth locations. Δx *is the center-to-center horizontal displacement distance while* sa_j *denotes the separated contiguous sub-aperture sections.*

WORK COMPLETED

Task 1 – FORA Measurements and Maintenance

During the LCAS 2015 experiment, PSU-ARL acted as the primary ship-based acoustic acquisition system. Acoustic data was collected for 14 days using the cardioid aperture of the FORA. A combined total of 1.7 TB of raw hydrophone data was collected in the interest of determining the effectiveness of CAS processing in the shallow-water littoral environment and comparison with PAS. Although several technical difficulties were encountered during this trial, in all, the FORA data collection system operated well during the experiment and the data was of very high quality. After the LCAS sea-trial the FORA system was shipped by ONR via NRL back to PSU-ARL for storage, maintenance, and repair of the FORA winch system as well as deck cable fiber communication lines

which were cut and spiced in the field during the LCAS 2015 trial. A portion of the funds within this grant went towards post-trial cleanup and preparation of the FORA system for the required repairs to both the winch and fiber optic communications lines. The FORA acquisition system was stored and faulty components within the winch system were localized and bids were requested for an overhaul of the entire winch motor and electrical system from several companies. Electric Motor & Supply (EMS) in Altoona, PA was contracted to complete a full system overhaul of the winch control cabinet and Breon's Inc. of Pleasant Gap, PA was contracted to overhaul the 440V, 3-phase winch motor system. Repairs to the winch system and fiber optic communications lines went well and the system was ready in time for the ONR-OA Seabed Characterization Experiment (SCEX) which took place in March/April, 2017.

Task 2 – Data Analysis

Analysis work began necessarily by updating John Preston's reverb processing system (RPS) to operate on LCAS PAS and CAS data. Cardioid beamforming algorithms used were developed using methods developed by Haralabus and Baldacci[5,6] as well as Hughes[7]. The LCAS dataset was then search using polar plots of range-normalized match filtered intensity for regions with clutter events of interest as well as the echo repeater (ER) target used during the LCAS experiment. Figure 3 shows an example of a range normalized match filtered return containing the echo repeater, biologic clutter, and static bottom clutter.

By creating movies of the matched filter polar plots, temporal dynamics between pings were be used to distinguish biologics from static bottom clutter. K-distribution shape parameter and correlation surface estimates were then calculated for pings of significant interest. Figure 4 shows a comparison of these two parameters for the idea case of the ER return (left) and boundary returns (right). The top two plots display the level of the match filtered acoustic return with a windowed range segment between black bars. These range segments was used to calculate shape parameter and correlation surface estimates in the underlying plots. Comparing the K-distribution shape parameter estimate, α, and the correlation surface of boundary returns to echo repeater returns shows how each of these metrics are effected by the target presence. While the shape parameter drops significantly for a windowed region near the target ($\alpha < 5$) the correlation surface widens significantly. When the return contains only boundary backscattering the shape parameter grows ($\alpha > 10$) and the correlation surface converges to the ideal surface determined by the array beamform and apodization function.[4] Note in this particular comparison it was found that alpha parameters less than $\alpha = 5$ were generally highly non-Rayleigh in nature.

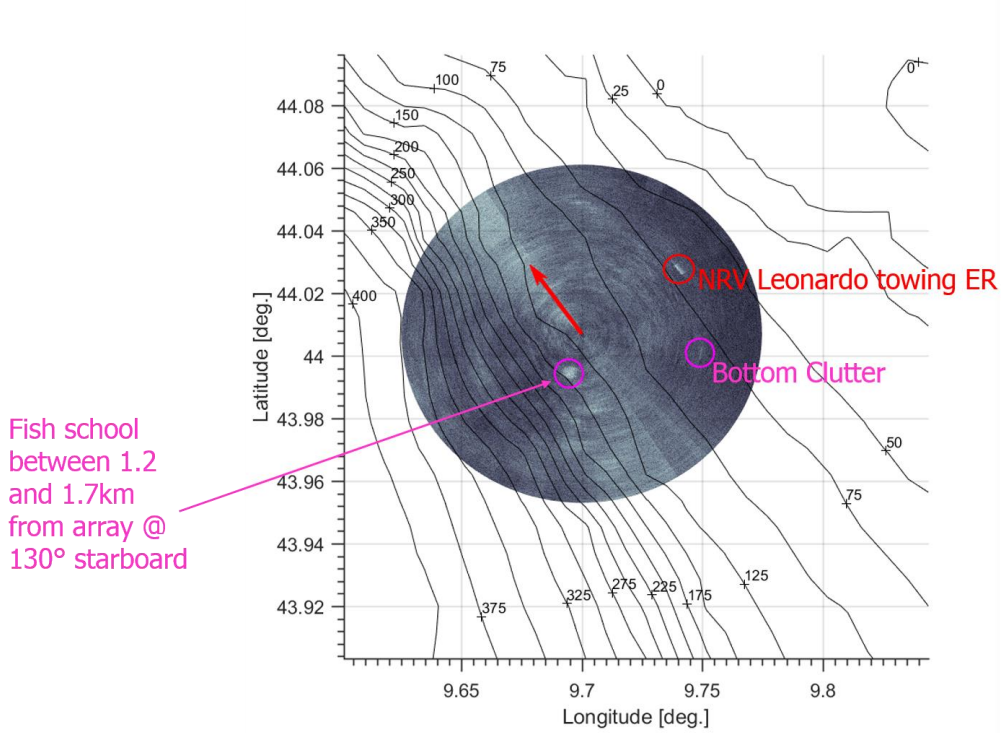

Figure 3: Polar plot of the range-compensated match filtered acoustic data translated to latitude and longitude. Color scale of ±30dB. These figures were used to find data that contained biologic and static bottom clutter as well as echo repeater returns. Temporal dynamics between pings were used to separate biologic and bottom clutter.

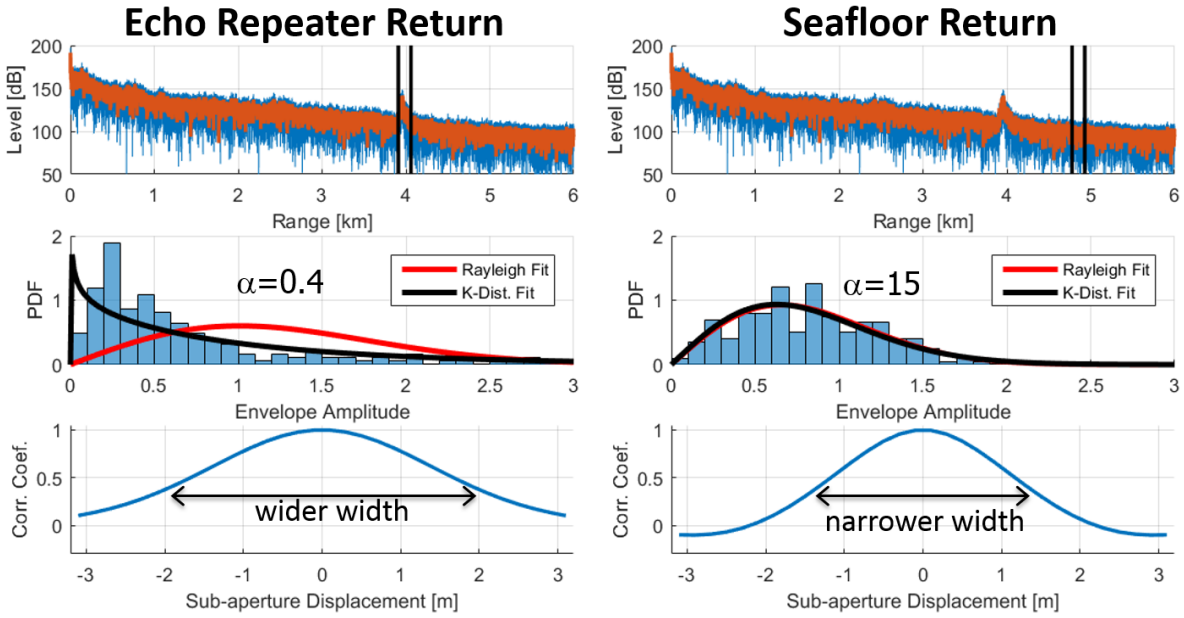

Figure 4: This figure shows the level of the acoustic return in the top plot with a particular range-window shown between black vertical bars. This range-window was used to estimate the underlying plot's statistics. Note the K-distribution (black curve) shape parameter, α, lessens significantly for the echo repeater return and grows toward the Rayleigh fit (red curve) limit for boundary returns. Also note the correlation surface widens significantly when estimated for the echo repeater return compared to seafloor and surface returns.

To assess how these two metrics are related to boundary clutter, volume clutter, and target returns, geographically (lat./lon.) registered polar plots were created using shape parameter and aperture coherence (Eq. 2). Although there are other methods of parametrizing the correlation surface (such as looking at the surface width as demonstrated in Figure 4) using this simple averaging method limits the correlation information across the aperture to a single value between 0 and 1 and can be used as a masking function similar to methods used by Blomberg et. al.[8] Figure 5 shows a polar plot of the shape parameter using the same PAS sonar ping used for the matched filtered return in Figure 2. The color scale in this figure has been inverted so very low shape parameter regions (highly non-Rayleigh) are shown as bright features. Notice that the echo repeater return and static bottom clutter are bright in each of these figures in addition to many regions of clutter. Some regions of the fish school also show up brightly but there is significant spatial variation within the school compared to the match filtered return shown in Figure 2.

Figure 6 also uses the same sonar ping data but the shape parameter has now been masked (multiplied by) the 0-1 normalized aperture coherence (Eq. 2) in order to emphasize regions of high spatial signal coherence. The echo repeater return and bottom clutter are still bright in each of these figures but their location has been refined. Additionally, the impact of the fish school has been greatly reduced.

To compare this processing method for PAS and CAS, figures similar to Figures 5 and 6 were created using CAS data that was recorded simultaneously. In this work a 20 second length CAS pulse was processed similar to the 1 second length PAS pulse to give a limiting example of the effects of temporal pulse coherence on the shape parameter estimate as well as the spatial horizontal array correlation. Figures 7 and 8 show the CAS shape parameter and the shape parameter masked (multiplied by) the 0-1 normalized aperture coherence of the CAS pulse. Notice that the echo repeater return and static bottom clutter still appear to have very low shape parameter values (brighter regions are low in value). However, there is far more clutter in the CAS shape parameter data (Figure 7) than the PAS shape parameter data (Figure 5). Some of this additional clutter may be mitigated by adjusting K-distribution estimation parameters and threshold values, however, for this comparison these parameters were kept consistent for PAS and CAS to provide a comparison of changes caused only by aperture coherence masking. Figure 8 shows the results of using aperture coherence masking in addition to shape parameter estimation. Note the target remains highly visible while the visibility of the bottom clutter is slightly minimized due to the movement of the measurement vessel and the longer temporal averaging window of the CAS pulse. Also note the impact of the fish school and other clutter has been drastically reduced compared to Figure 7.

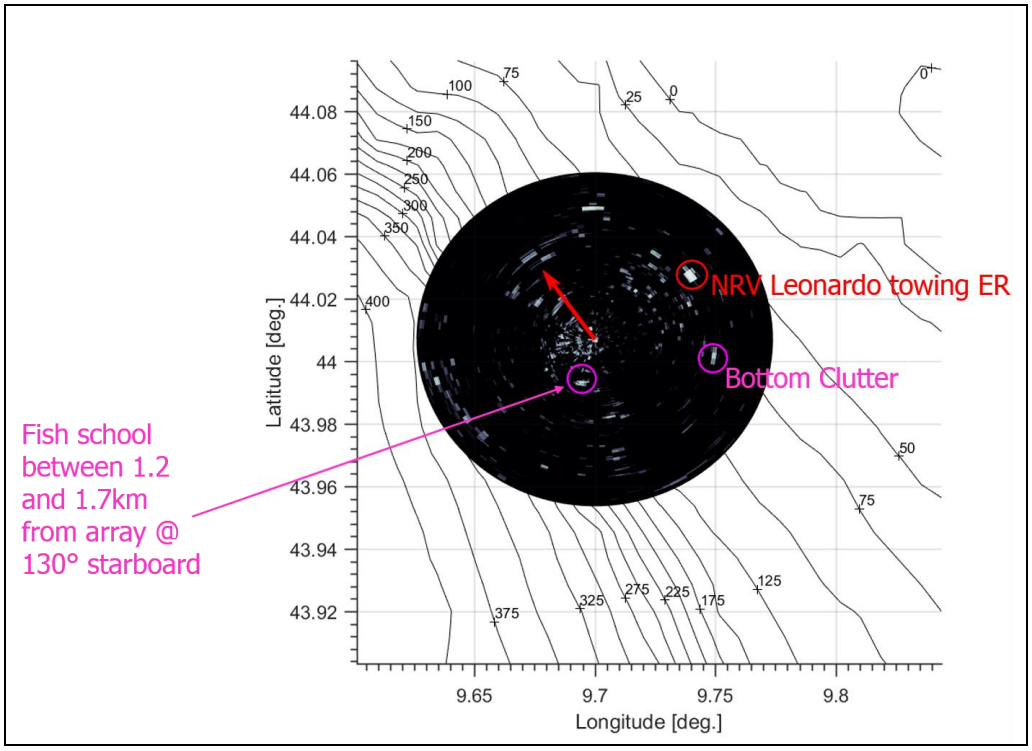

Figure 5: Polar plot of PAS K-distribution shape parameter. 5-0 color scale (dark areas are >5 and considered Rayleigh-like for this work). Note the strongly non-Rayleigh returns from the ER and the stationary bottom clutter as well as the irregular spatial variation of the fish school.

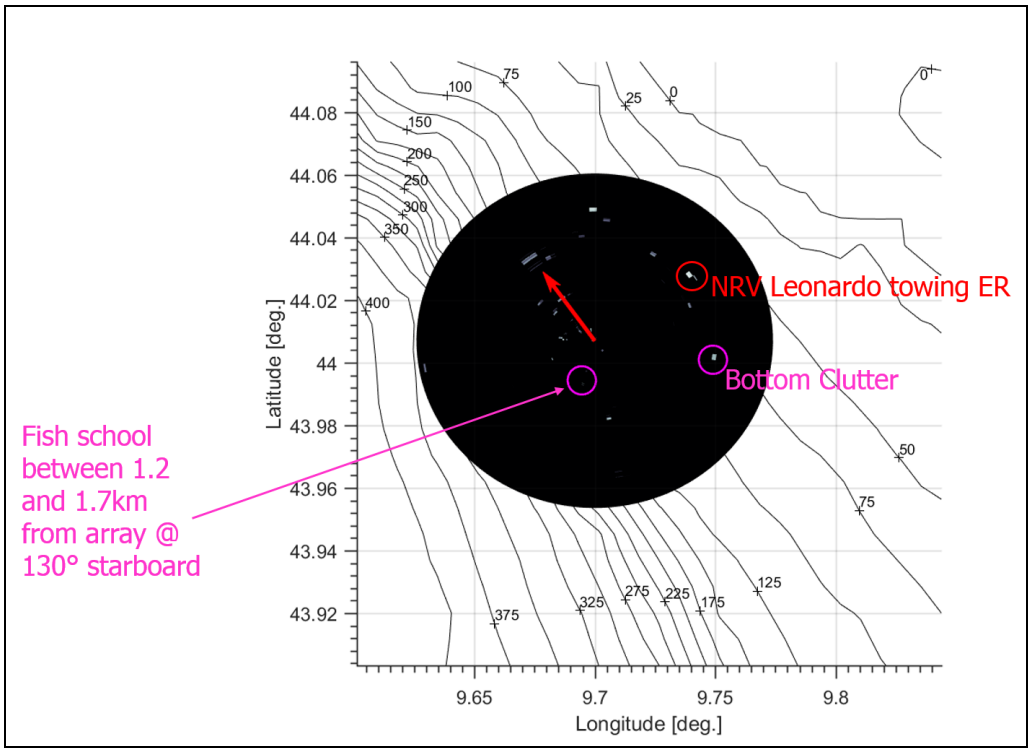

Figure 6: Polar plot of PAS K-distribution shape parameter masked using aperture coherence. 5-0 color scale (dark areas are >5 and considered Rayleigh-like for this work). Note the ER and bottom clutter still have strongly non-Rayleigh returns and may be more refined geographically. However, much of the effects of the fish school and other boundary clutter has been reduced.

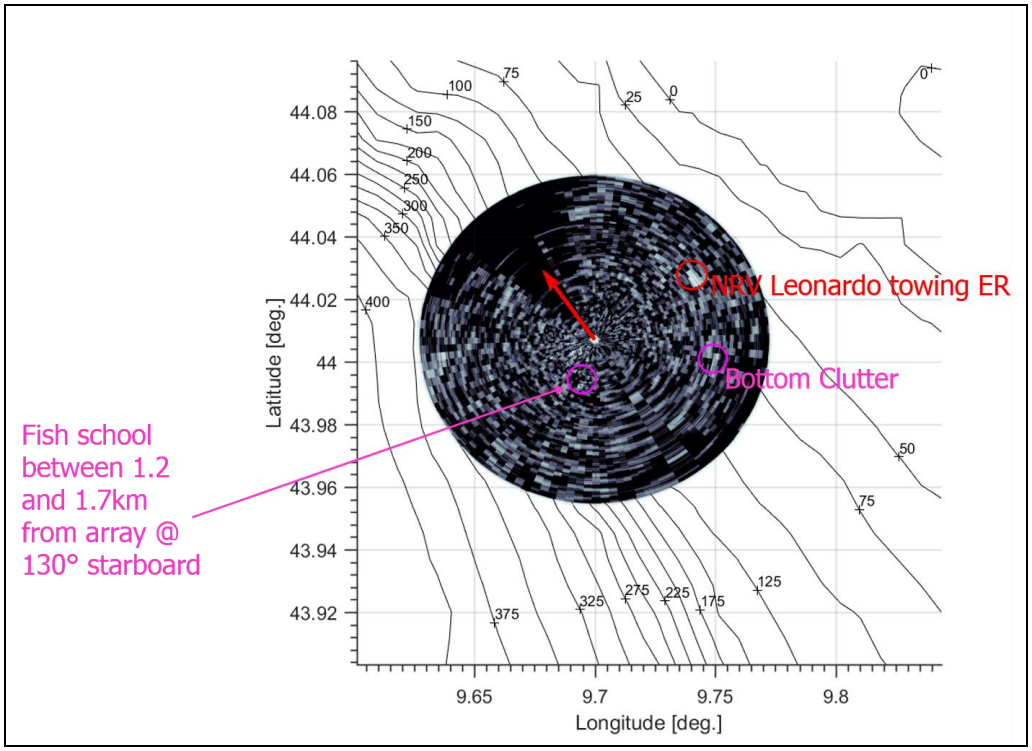

Figure 7: Polar plot of CAS K-distribution shape parameter. 5-0 color scale (dark areas are >5 and considered Rayleigh-like for this work). Note the strongly non-Rayleigh returns from the ER and the bottom clutter as well as the irregular spatial variation of the fish school.

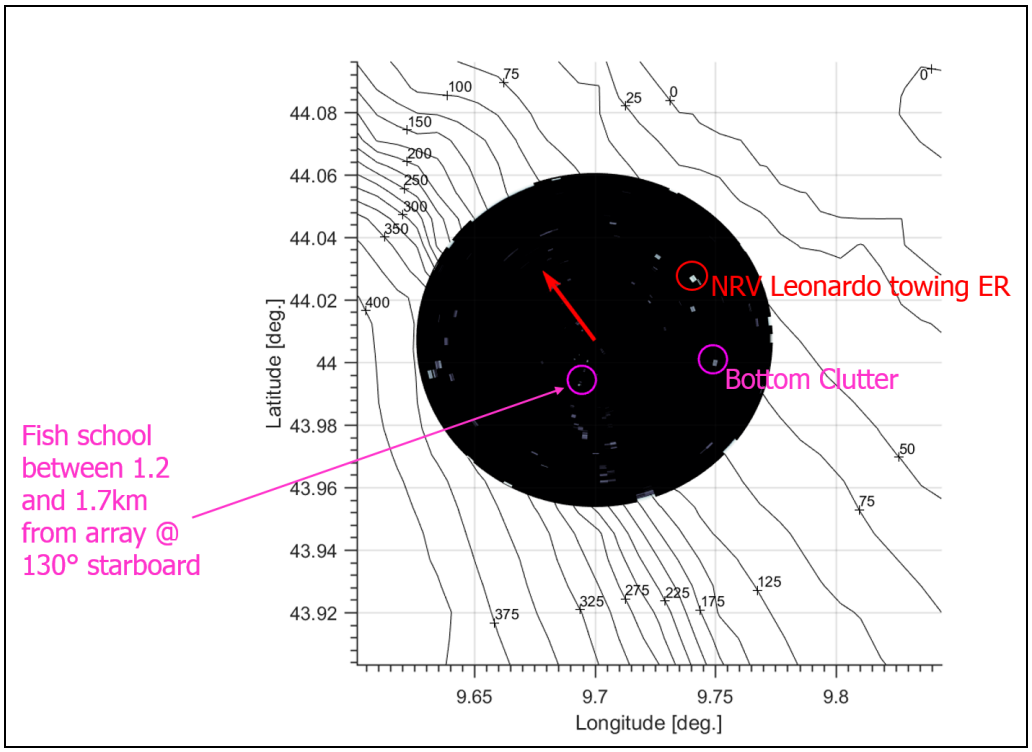

Figure 8: Polar plot of CAS K-distribution shape parameter masked using aperture coherence. 5-0 color scale (dark areas are >5 and considered Rayleigh-like for this work). Note the ER and bottom clutter still have strongly non-Rayleigh returns and are more refined geographically. The bottom clutter return has also been reduced slightly. Much of the effects of the fish school and other boundary clutter has also been reduced.

The color scaling of Figures 5-8 were chosen carefully using the data shown in Figure 9. This figure shows a scatterplot of K-distribution shape parameter vs. aperture coherence using shallow broadside returns from 12 consecutive pulses. This figure explains why using these two metrics in tandem may provide a more stable Rayleighness estimation than using either singly. Looking at Figure 9, there does not appear to be any direct correlation (scatter plot correlation in this case, or linear dependence) between these two metrics— this would show up in the scatterplot as positively or negatively sloped pattern within the scatterplot. However, while there is no direct correlation between the two, high values of aperture coherence do often imply low values of shape parameter. This may imply that, as assumed in the initial thesis of this work, these parameters both provide information about the Rayleigh-like nature of the return data through significantly differing methods. The spatial correlation and aperture coherence provide information about the geometric parameters of the wave front which can be assumed more broad for a non-Rayleigh return, while the K-distribution provides information about the temporal characteristics of the return intensity. Using Figure 9, returns with $\alpha<5$ and AC>0.7 were assumed highly non-Rayleigh returns.

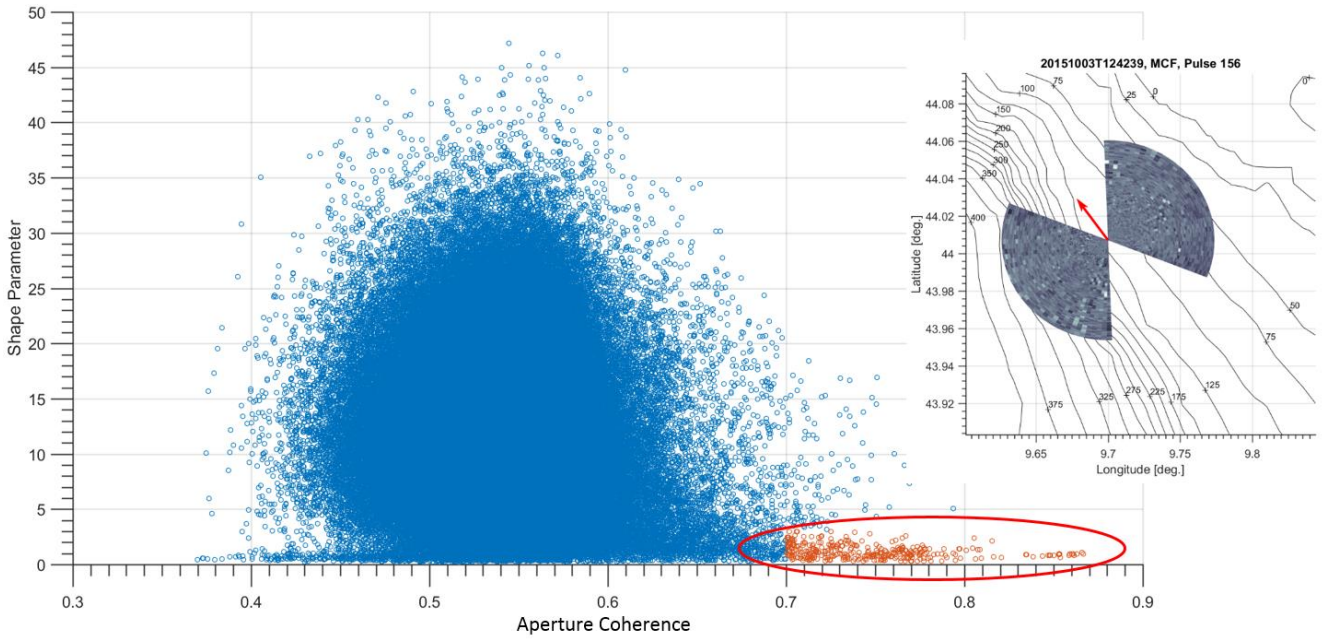

*Figure 9: Scatterplot of K-distribution shape parameter vs. aperture correlation for 12 PAS pulses ±60° of broadside. The red circle and orange marker show the region where both shape parameter and aperture correlation show highly non-Rayleigh returns. Polar plot in the upper right of figures displays the regions used to create scatterplot. Note that the polar plot was place so it **does not** cover any scatterplot data points.*

Figures 10 and 11 give another interesting comparison of PAS and CAS processing, again using the 1 second PAS and 20 second CAS pulse as a limiting example. These figures show the aperture correlation verse processing window (effectively range) for an azimuth containing only boundary scattering (Figure 10) and azimuth containing the echo repeater return (Figure 11). The mean aperture coherence in both figures remains relatively stable just under 0.5 while the instantaneous level of the PAS and CAS coherence from boundary scattering varies significantly from one another. In Figure 11, it is evident that both PAS and CAS capture the significant broadening of the spatial correlation surface of the echo repeater return circled in black. Also interesting is the higher level and longer range-duration of CAS coherence even though the bandwidth-product of the two signals is similar. This may signify a significant advantage to the longer signal duration used in CAS and should be investigated further.

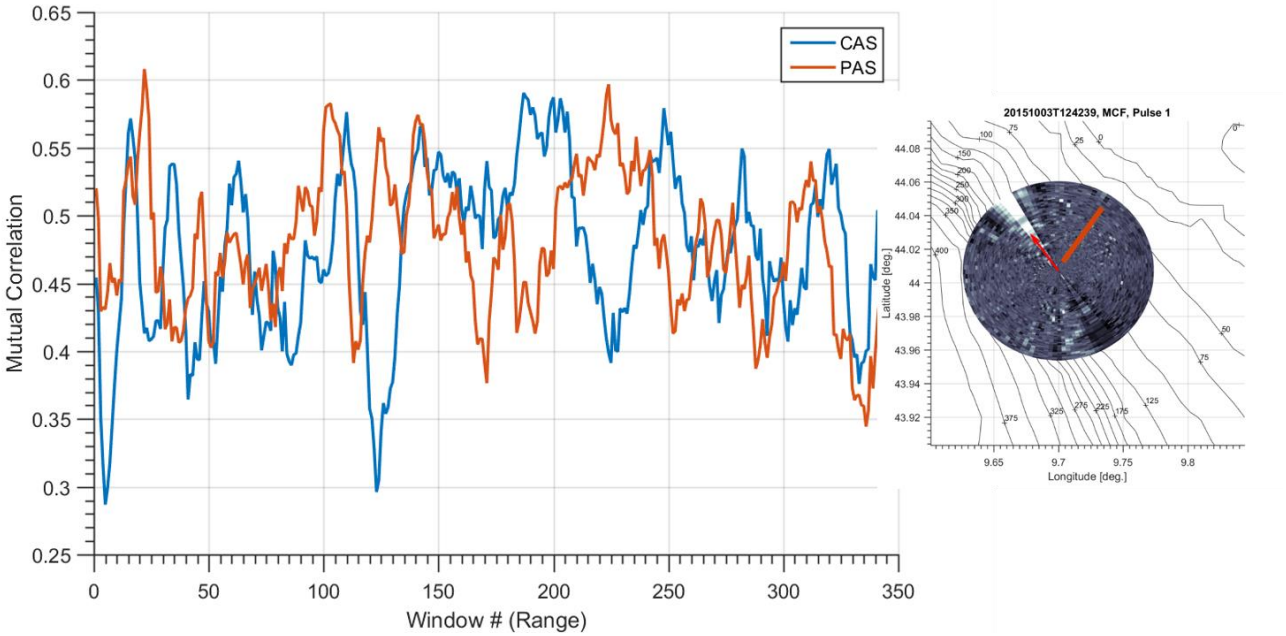

Figure 10: Aperture correlation verse processing window (effectively range) for an azimuth containing only boundary scattering. Mean aperture coherence remains relatively stable (just under 0.5) for both PAS and CAS coherence while the range values from boundary scattering can vary from one another.

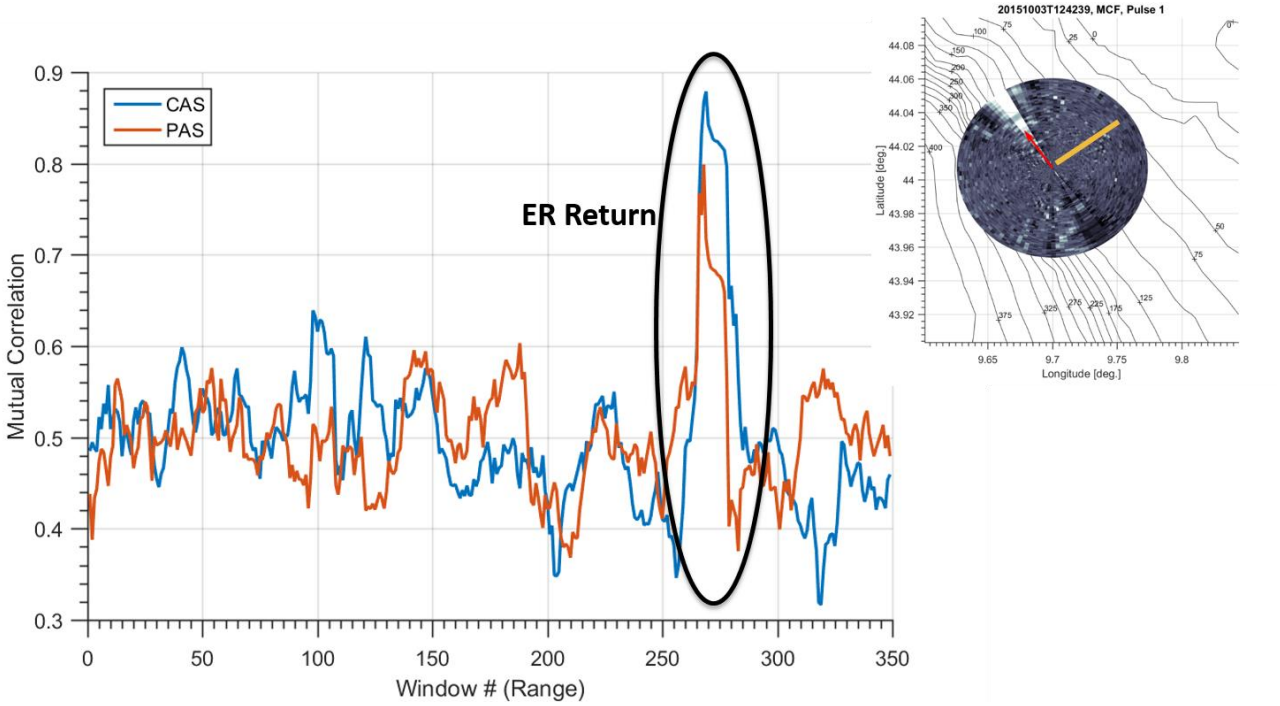

Figure 11: Aperture correlation verse processing window (effectively range) for an azimuth containing echo repeater return. Mean aperture coherence remains relatively stable (just under 0.5) for both PAS and CAS coherence and both pulse types show a large increase in the aperture coherence of the echo repeater return. Also interesting is the higher level of the CAS aperture coherence as well as longer range-duration even though the bandwidth-product of the two signals is similar.

RESULTS

Data collected during the 2015 LCAS experiment was used in an early effort to understand the utility of using spatial correlation for classification in addition to backscattered intensity distributions (such as the K-distribution) for long-range sonar. This work provides a first look at both the additional information that spatial correlation may provide for sonar classification and a comparison of this metric using PAS and CAS. Figures 5-8 show the improvement that using the averaged horizontal spatial correlation as a mask for the K-distribution shape parameter may provide, and along with the scatterplot comparison in Figure 9, show that there is additional quantifiable information in this metric. The use of the aperture coherence as an analytic mask appears to lessen the effects of randomly distributed high shape parameter values (random clutter) as well as a fish school return by limiting these values to those returns of broad spatial coherence.

Although this work focused on using spatial coherence in conjunction with commonly used intensity distributions to improve clutter rejection, there may be utility in using this metric for detection itself. Figure 11 shows the response of this metric to an echo repeater target and the possible benefits of using high duty cycle signals in this geometry. This work has shown imperially that even at long ranges spatial correlation statistics can display significant differences between boundary returns, volume clutter, and target events and may provide useful classification information after careful characterization.

Future work should include a more thorough empirical comparison of clutter and target events using not only aperture coherence but also the detailed shape and transition (change in surface shape over time) of the spatial correlation surface. This will likely provide an understanding of the dependence of the spatial correlation surface on scatterer structure and the surrounding environment. Development of a physics-based long-range model capable of modeling environmental influence as well as scatterer structure (likely requiring a hybrid model) would allow the researchers to more fully understand the importance of environmental parameters and model key clutter and target events. Further processing and comparison of the clutter rejection properties of this metric should be investigated for a wide range of pulse lengths to understand the impact of temporal coherence and determine the utility of CAS vs. PAS. Finally, applying this processing and modeling methods to a close-range dataset with far less environmental parameters may provide additional incite towards interpreting the underlying physics from these measurements.

IMPACT

Volume and boundary clutter are very real operational difficulties for the fleet, especially within the shallow-water littoral environment. Development of processing methods for improved classification and mitigation of clutter is key to lessening false alarm rates for CFAR and other sonar processing systems.

The experimental work undertaken by the FORA team during the LCAS experiment provided a wealth of data for many researchers in the interest of CAS performance and processing. This research may provide improved understanding of the advantages and disadvantages of CAS verse PAS.

The cardioid array technology that the FORA system offers provides novel improvements in towed array data collection by greatly lessening the effects of ambiguous arrivals of traditional line arrays. The processing algorithms designed during this work may provide a baseline for future naval applications.

RELATED PROJECTS

Analysis of Spatiotemporal Clutter Statistics and Support of the Five Octave Research Array
Grant Number: N00014-16-1-2561, PI: Chad Smith

Statistical clutter characterization and support for the Five Octave Research Array.

The previously mentioneded multi-national joint research project (MN-JRP) lead by the Centre for Maritime Research and Experimentation (CMRE). This MN-JRP was designed to assess the utility and nuances of using high duty cycle sonar for ASW.

PUBLICATIONS

Smith, C., & Preston, J. (2017, June). Observations of non-Rayleigh acoustic backscatter and spatial correlation. *The Journal of the Acoustical Society of America*. *To be presented June 25th, 2017.*

Smith, C., & Preston, J. (2017, June). Observations of non-Rayleigh acoustic backscatter and spatial correlation. In *Proceedings of Meetings on Acoustics 173 ASA. In prepration.*

REFERENCES

[1] Ward, K. D., Watts, S., & Tough, R. J. (2006). *Sea clutter: scattering, the K distribution and radar performance* (Vol. 20). IET.

[2] Weinberg, G. V. (2016). Error bounds on the Rayleigh approximation of the K-distribution. *IET Signal Processing*, *10*(3), 284-290.

[3] Brown, D. C., Lyons, A. P., Cook, D. A. (2014). Spatial coherence theory and its application to synthetic aperture systems. *Proceedings of the Institute of Acoustics*, September 2014.

[4] Jackson, D. R., & Moravan, K. Y. (1984). Horizontal spatial coherence of ocean reverberation. *The Journal of the Acoustical Society of America*, *75*(2), 428-436.

[5] Haralabus, G., & Baldacci, A. (2006, September). Unambiguous triplet array beamforming and calibration algorithms to facilitate an environmentally adaptive active sonar concept. In OCEANS 2006 (pp. 1-6). IEEE.

[6] Baldacci A., Haralabus G., and Velzen M. (2006, August). Cardioid receive array calibration for active systems, NURC Reprint Series: NURC-PR-2006-015.

[7] Hughes, D. T. (2000). Aspects of cardioid processing (No. SACLANTCEN-SR-329). SACLANT Undersea Research Centre, La Spezia, Italy.

[8] Blomberg, A. E. A., Nilsen, C. C., Austeng, A., & Hansen, R. E. (2013). Adaptive sonar imaging using aperture coherence. *IEEE Journal of Oceanic Engineering*, *38*(1), 98-108.

[9] Abraham, D. A., & Lyons, A. P. (2010). Reliable methods for estimating the K-distribution shape parameter. IEEE Journal of Oceanic Engineering, 35(2), 288-302.

[10] Redding, N. J. (1999). Estimating the parameters of the K distribution in the intensity domain.

[11] Cox, H. (1973). Line array performance when the signal coherence is spatially dependent. *The Journal of the Acoustical Society of America*, *54*(6), 1743-1746.

[12] Zhang, Z. Y. (2009). Estimating sonar system losses due to signal spatial decorrelation. *Proceedings of ACOUSTICS 2009*, Australian Acoustical Society, Adelaide, Australia.

[13] Lynch, J. F., Duda, T. F., Colosi, J. A. (2014). Acoustical Horizontal Array Coherence Lengths and the "Carey Number". *Acoustics Today*, winter 2014.

[14] Green, Michael C. (1976). Gain of a linear array for spatially dependent signal coherence. *The Journal of the Acoustical Society of America*, 60, 129-132.

[15] Abraham, D. A., & Lyons, A. P. (2002). Novel physical interpretations of K-distributed reverberation. *IEEE Journal of Oceanic Engineering*, *27*(4), 800-813.

[16] Chang, E., & Tinkle, M. D. (2001). Coherence of pulsed signal and implications to synthetic aperture sonar processing. In *OCEANS, 2001. MTS/IEEE Conference and Exhibition* (Vol. 1, pp. 193-201). IEEE.
[17] Urick, R. J. (1983). *Principles of underwater sound for engineers*. 3rd edition. Tata McGraw-Hill Education.
[18] Fattaccioli, D., Cristol, X., Destelan, G. P., & Danet, P. (2009). Sonar processing performance in random environments. *Congrès Underwater Acoustics Measurements (UAM 09), Nafplion, Grèce*, 21-26.
[19] J. R. Preston, K. M. Becker, P. Shultz and J. McIlvain, "An overview and lessons learned from the five octave research array (FORA) and some perspectives for future towed arrays," 4th International Conference on Underwater Acoustic Measurements: Technologies and Results, Kos, Greece, June 2011 (Invited).
[20] J. R. Preston, "Using triplet arrays for reverberation analysis and inversions," IEEE J. Oceanic Engineering, 32, 879-896, 2007.
[21] K. M. Becker and J. R. Preston, "The ONR Five Octave Research Array (FORA) at Penn State," Oceans 2003 Proceedings, San Diego, CA, September 2003.